Valorization of Municipal Biowaste into Electrospun Poly(3-hydroxybutyrate-co-3-hydroxyvalerate) Biopapers for Food Packaging Applications

Beatriz Meléndez-Rodríguez[1], Sergio Torres-Giner[1]*, Laura Lorini[2], Francesco Valentino[2], Chris Sammon[3], Luis Cabedo[4], and José María Lagarón*

[1] Novel Materials and Nanotechnology Group, Institute of Agrochemistry and Food Technology (IATA), Spanish Council for Scientific Research (CSIC), Paterna, Spain

[2] Department of Chemistry, "La Sapienza" University of Rome, Rome, Italy

[3] Materials and Engineering Research Institute, Sheffield Hallam University, Sheffield, United Kingdom

[4] Polymers and Advanced Materials Group (PIMA), Universitat Jaume I (UJI), Castellón, Spain

Abstract: The present study reports on the production and characterization of a new biopackaging material made of poly(3-hydroxybutyrate-*co*-3-hydroxyvalerate) (PHBV) derived from municipal biowaste (MBW) and produced by the mixed bacterial culture technology. After purification and extraction, the MBW-derived PHBV was processed by electrospinning to yield defect-free ultrathin fibers, which were thermally post-treated. Annealing at 130 °C, well below the biopolymer's melting temperature (T_m), successfully yielded a continuous film resulting from coalescence of the electrospun fibrillar morphology, the so-called biopaper, exhibiting enhanced optical and color properties compared to traditional melt compounding routes. The crystallinity and crystalline morphology were comprehensively studied as a function of temperature by attenuated total reflectance-Fourier transform infrared (ATR-FTIR) spectroscopy and combined time-resolved synchrotron small- and wide-angle X-ray scattering (SAXS and WAXS) experiments, which clearly indicated that the molecular order within the copolyester was improved up to a maximum at 130 °C, and then it decreased at the biopolymer's T_m. It was hypothesized that by annealing at the temperature at which the thermally induced molecular order is maximized, the fibers generated sufficient mobility to align alongside, hence reducing surface energy and porosity. The data suggest that this material shows a good balance between enhanced mechanical and improved barrier properties to vapors and gases in comparison to traditional paper and other currently used petroleum-derived polymers, thus presenting significant potential to be part of innovative food biopackaging designs for the protection and preservation of foods in a circular bioeconomy scenario.

Keywords: PHBV; electrospinning; biopapers; waste valorization; food packaging; circular bioeconomy

1. Introduction

The potential of polyhydroxyalkanoates (PHAs) as biobased and biodegradable replacements for conventional bulk commodity plastic packaging while promoting sustainable development has long been recognized (Koller 2014). These biopolymers are mainly produced by the action of bacteria, both Gram-positive (G+) and Gram-negative (G−) (Rehm 2003), during the fermentation of sugar or lipids under famine conditions (Saharan, Grewal, and Kumar 2014). However, there is also an increasing number of archaea that are being used to produce PHAs (Koller et al. 2017). The most studied PHA is poly(3-hydroxybutyrate) (PHB). The homopolyester shows thermal and mechanical properties similar to those of petrochemical polyolefins such as low-density polyethylene (LDPE) and polypropylene (PP) (Kourmentza and Kornaros 2016, Torres-Giner, Montanes, et al. 2018). However, its low ductility and toughness as well as its narrow processing window limit the use of PHB for packaging. For this reason, poly(3-hydroxybutyrate-*co*-3-hydroxyvalerate) (PHBV), that is, its copolymers with 3-hydroxyvalerate (3HV), shows reduced crystallinity and decreased stiffness, having also a lower melting temperature (T_m), which makes it a more interesting candidate in the areas of biodegradable packaging (Sängerlaub et al. 2019).

Current manufacturing processes of PHAs by bacterial fermentation involve fermentation, isolation, and purification from the fermentation broth (Acevedo et al. 2018, Fabra, Lopez-Rubio, and Lagaron 2014). Much effort and improvements are currently being made to reduce fermentation and downstream processing costs (Laycock et al. 2013), which are on the order of up to 15 times higher than for conventional polyolefins (Choi and Lee 1997). In this regard, the synthesis of PHAs produced by mixed microbial cultures (MMCs) using biowaste as feedstock, such as industrial waste and food processing by-products, can make its industrial production more competitive (Reis et al. 2011). In fact, pure culture systems based on refined feedstock and sterile cultivation conditions contribute the most to the PHA production cost (Fernández-Dacosta et al. 2015). Furthermore, the valorization of by-products and wastes is environmentally attractive in a more sustainable circular bioeconomy scenario (Gurieff and Lant 2007). In this regard, different organic wastes have been used as substrates to produce PHAs, for instance molasses (Albuquerque, Torres, and Reis 2010), olive and palm oil mill effluent (Dionisi et al. 2005, Hassan et al. 1997), fermented fruit waste (Melendez-Rodriguez et al. 2018), and cheese whey (CW) (Colombo et al. 2016).

Municipal waste, wastewaters, and the organic fraction of municipal solid waste (OFMSW) also show great potential as the feeding solution for PHA production. However, to date, few studies have shown the use of OFMSW for the production of these biopolymers (Morgan-Sagastume et al. 2015). Along with the production of biogas, the most common processes applied for biological sludge disposal, to stabilize organic matter and valorize different substrates into added-value marketable products, are composting and anaerobic digestion (Mata-Alvarez et al. 2014). Other research works have demonstrated that the use of OFMSW during the accumulation step led to improved PHA productivity (Korkakaki et al. 2016). Another study demonstrated that the PHA accumulation fed with fermentation volatile fatty acids (VFAs) that were obtained from food wastes and excess sludge was higher than the one produced with analytically pure VFAs (Zhang, Wu, and Chen 2014). PHA production was also reported utilizing MMC indigenous to an activated sludge process on carbon present in municipal wastewaters (Coats et al. 2007). Therefore, the integration of the so-called MMC–PHA production in this kind of

infrastructure using activated sludge as an inoculum can make this technology more economically and environmentally sustainable.

Electrospinning is an innovative processing technology that allows the formation of continuous polymer fibers, with diameters ranging from several nanometers to a few microns, by virtue of high voltage (Doshi and Reneker 1995). Both the solution properties, such as surface tension, viscosity, and conductivity, and the processing conditions, such as flow rate, voltage, and injector-to-collector distance, are known to impact size, size distribution, and morphology of the resultant fiber mats. The formation of fiber-based continuous films of reduced porosity, called biopapers, can be achieved by annealing the electrospun mats and the resultant coalescence and rearrangement of the nanofibers in the material to reduce surface tension (Cherpinski et al. 2017, Melendez-Rodriguez et al. 2018). The term biopaper refers to electrospun fiber-based material concepts made of biopolymers that, unlike conventional paper made of cellulose that involves severe chemical processes and contains petrochemical additives and/or hydrophobizing coatings, are fully functional in terms of physicochemical properties, biobased, and biodegradable. The term biopaper has also been coined in connection to biomaterials that serve as flat scaffolds and contain electrospun biopolymers, in which cells are printed onto each sheet in a two-dimensional (2D) pattern, and then the biopapers are stacked to generate a three-dimensional (3D) structure (Pal, Banthia, and Majumdar 2009). Biopapers make the use of electrospun PHA a very interesting alternative in the packaging industry since continuous and handable films can be obtained with minimal thermal exposure that can exhibit improved optical and mechanical strength as well as flexibility with excellent water resistance and gas and vapor barrier properties (Cherpinski, Torres-Giner, Cabedo, et al. 2018). Moreover, electrospinning allows for the incorporation of functional additives into the biopolymers and, thus, the formation of coatings or interlayers of interest in active and bioactive packaging (Alp-Erbay et al. 2019, Cherpinski, Gozutok, et al. 2018, Hu et al. 2018, Lasprilla-Botero et al. 2018, Quiles-Carrillo et al. 2019a, Spagnol et al. 2018).

The objective of this study was to valorize, for the first time, typical municipal biowaste streams into biopapers of PHBV produced by thermal post-treatment of electrospun mats and then asses the resulting morphology, crystallinity, and crystalline morphology as a function of temperature and their final physicochemical properties relevant for food biopackaging applications.

2. Experimental Section

2.1. Materials

The municipal biowaste (MBW) PHBV was produced at the pilot platform in the Treviso Municipal Wastewater Treatment Plant (Treviso, Italy), from a feedstock composed of a mixture of liquid slurry resulting from squeezing OFMSW and biological sludge from the treatment of urban wastewater. The commercial PHBV used for comparison was ENMAT Y1000P, which was produced by Tianan Biologic Materials (Ningbo, China) and supplied by Ocenic Resins S.L. (Valencia, Spain). According to the manufacturer, the 3HV fraction in the commercial copolyester is 2–3 mol %.

2,2,2-Trifluoroethanol (TFE), ≥ 99 % purity, 1-butanol, reagent grade with 99.5 % purity, methanol, sulfuric acid (H_2SO_4), benzoic acid, and d-limonene, 98 % purity, were all purchased from Sigma-Aldrich S.A. (Madrid, Spain). Chloroform, stabilized with ethanol and 99.8 % purity, was obtained from Panreac S.A. (Barcelona, Spain).

2.2. Production

The PHBV production consisted of three process steps using the fermented mixture of OFMSW and biological sludge. In the first stage, the precursors for PHA biosynthesis, that is, VFAs, were produced in an anaerobic fermentation reactor of 380 L. Then, biomass cultivation was carried out in a second aerobic reactor of 100 L, referred to as the sequencing batch reactor (SBR). Finally, for achieving PHA accumulation within the cellular cytoplasm, a third fed-batch aerobic reactor of 70–90 L was used. At the end of the accumulation step, the PHA concentration reached up to a value of 2.0–2.5 g/L, corresponding to a maximum PHA content of 50–60 % of cell dry weight, that is, the mass ratio of PHA vs volatile solids. This PHA-rich raw biomass was collected following a protocol addressed to the long-term PHA conservation inside the cells before the extraction/purification steps. In this protocol, once each accumulation was completed, the PHA-rich biomass was left to settle under gravity and, thereafter, the thickened slurry was centrifuged for 15 min at 4500 rpm in a Heraeus Megafuge 40 Centrifuge with a Swinging Bucket Rotor (maximum radius: 195 mm; minimum radius: 83 mm) from Thermo Fisher Scientific (Waltham, MA). Finally, the wet pellet was pretreated for 15 min at 145 °C and then dried at 60 °C overnight. A more detailed description of the production process can be found in the research study of Valentino et al. (Valentino et al. 2019).

2.3. Extraction and Purification

The unpurified PHBV was extracted using the chloroform-based extraction method reported previously (Fiorese et al. 2009). This purification method involves a solvent, which requires to be evaporated. While at the lab scale this possesses no relevant issues, evaporation methods of organic solvents are hardly applicable at an industrial scale, specially under sustainable manufacturing practices. In this regard, the consumption of large amounts of organic solvents can be avoided by “antisolvents”, that is, solvents in which the respective PHA is nonsoluble and precipitates (Madkour et al. 2013). To do this, the PHA solution must be mixed with a large volume of the nonsolvent, yielding a mixture of at least two different solvents in which PHA precipitates (Griffin 1994). Thereafter, the precipitated PHA can be separated from the solvent mixture by centrifugation or filtration and, at the large scale, the organic solvent could be recovered by separation techniques and reused for subsequent extraction processes. Furthermore, if water is used as the antisolvent, the sustainability of the process is improved (Li et al. 2015).

In this case, the MBW-derived PHBV was dissolved at 5 wt % in chloroform and the mixture was stirred at 50 °C for 24 h to degrade the non-PHA cellular material. Next, the solution was transferred to centrifugation tubes in which distilled water was added at 50 wt %. After manual shaking of the tubes, these were centrifuged for 5 min at 4000 rpm in an Avanti J-26S XP Centrifuge with a JLA-16.250 Rotor (maximum radius: 134 mm; average radius: 90 mm; minimum radius: 46 mm) from Beckman Coulter, Inc. (Brea, CA). Finally, the PHBV suspension

was recovered as sediment in the tubes with a pipette and transferred to beakers, leaving them in the extractor hood until the solvent was completely evaporated.

2.4. 3HV Content Determination

A powder sample of 3.5 mg was suspended in 2 ml of acidified methanol solution (3 % v/v H_2SO_4), containing benzoic acid at 0.005 % w/v as the internal standard, and 1 ml of chloroform in a screw-capped tube. Acid-catalyzed methanolysis occurred, and the 3-hydroxyacyl methyl esters of PHA were quantified by gas chromatography in a GC-FID PerkinElmer 8410 from PerkinElmer, Inc. (Waltham, MA). The relative abundance of 3-hydroxybutyrate (3HB) and 3HV monomers was determined using as a reference standard of the commercial PHBV copolymer with a known 3HV content of 5 wt % (Sigma-Aldrich S.r.l., Milan, Italy). The resultant molar fraction of 3HV in the copolyester was approximately 10 wt %.

2.5. Characterization of Solutions

The powder resulting from the purification process was dissolved at 15 wt % in a mixture of chloroform and butanol 75:25 (w/w) under magnetic stirring for 24 h at 50 °C. A solution of commercial PHBV was also prepared by dissolving the biopolymer at 10 wt % in neat TFE. Prior to electrospinning, the viscosity, conductivity, and surface tension of the PHBV solutions were characterized in the same conditions as reported earlier (Torres-Giner et al. 2017). To this end, a rotational viscometer Visco BasicPlus L from Fungilab S.A. (San Feliu de Llobregat, Spain) equipped with a low-viscosity adapter (LCP), a conductivity meter XS Con6 from Lab-box (Barcelona, Spain), and an EasyDyne K20 tensiometer from Krüss GmbH (Hamburg, Germany) were respectively used. All of the measurements were taken at room temperature in triplicate.

2.6. Electrospinning Process

The PHBV solutions were electrospun using a Fluidnatek LE-10 lab equipment manufactured by Bioinicia S.L. (Valencia, Spain), which is equipped with a horizontally scanning single needle injector. The conditions for processing the MBW-derived PHBV were optimal at a flow rate of 6 ml/h, 22 kV of voltage, and 25 cm of needle-to-collector distance. In the case of the commercial PHBV, electrospinning was carried out using previously optimized conditions, that is, 6 ml/h, 20 kV, and 15 cm (Melendez-Rodriguez, Figueroa-Lopez, et al. 2019). All of the PHBV solutions were electrospun for 1.3 h at 25 °C and 40 % relative humidity (RH), and the manufactured mats were stored in a desiccator at room temperature and at 0 % RH in the dark for, at least, a week prior to being annealed.

2.7. Preparation of Biopapers

The resultant fiber mats of PHBV were thermally post-treated in a 4122-model press from Carver, Inc. (Wabash, IN). Annealing was performed across the temperature range from 80 to 150 °C, for 5 s and without applying pressure. The electrospun mats of commercial PHBV were annealed at

155 °C, also for 5 s, also without applying pressure (Melendez-Rodriguez, Figueroa-Lopez, et al. 2019). An average thickness of approximately 30 μm was attained for all of the thermally postprocessed samples. The samples were stored in a desiccator at 0 % RH for 2 weeks before subsequent characterization.

2.8. Characterization

2.8.1. Microscopy

The morphology of the samples was determined by scanning electron microscopy (SEM) using an S-4800 model from Hitachi (Tokyo, Japan) and applying an accelerating voltage of 10 kV. For cross-section observation, the materials were cryo-fractured by immersion in liquid nitrogen. Prior to observation, the samples were fixed to beveled holders by conductive double-sided adhesive tape and a mixture of gold–palladium was sputtered on their surface under vacuum. Dimensions were estimated using a minimum of 20 SEM micrographs in their original magnification with Aperture software from Apple (Cupertino, CA).

2.8.2. Transparency

The light transmission of biopapers was determined using 50 mm × 30 mm specimens in an ultraviolet–visible (UV–vis) spectrophotometer VIS3000 (Dinko Instruments, Barcelona, Spain). The absorption of light was quantified at wavelengths in the 200–700 nm range. Equations 1 (Shiku et al. 2004) and 2 (Kanatt et al. 2012) were followed to determine the values of transparency (T) and opacity (O), respectively

$$T = \frac{A_{600}}{L} \tag{1}$$

$$O = A_{500} \times L \tag{2}$$

in which A_{600} and A_{500} correspond to the absorbance values at 600 and 500 nm, respectively, whereas L represents the film thickness (mm).

2.8.3. Color

The color of the biopapers was estimated using a chroma meter CR-400 (Konica Minolta, Tokyo, Japan). Equation 3 (Arfat et al. 2017) was used to determine the color difference (ΔE^*) between the test sample and the control sample of commercial PHBV

$$\Delta E^* = [(\Delta L^*)^2 + (\Delta a^*)^2 + (\Delta b^*)^2]^{0.5} \tag{3}$$

in which ΔL^* represents the difference in terms of lightness from black to white, whereas Δa^* and Δb^* correspond to the differences in color, from green to red and blue to yellow, respectively. Color changes were assessed using a previous grading (Agüero et al. 2019).

2.8.4. Thermal Analysis

The main thermal parameters of the samples were determined by differential scanning calorimetry (DSC) with a DSC-7 tool from PerkinElmer, Inc. (Waltham, MA), equipped with the Intracooler 2 cooling accessory. Thermal runs consisted of a first heating step from −30 to 180 °C, a cooling step to −30 °C, and a second heating step to 200 °C. The runs were set to 10 °C/min using a sample amount of ∼3 mg and aluminum pans. The thermograms were corrected with an empty pan, and the equipment was calibrated with indium.

Thermogravimetric analysis (TGA) was carried out in a TG-STDA thermobalance TGA/STDA851e/LF/1600 from Mettler-Toledo, LLC (Columbus, OH). The heating program consisted of a ramp from 50 to 900 °C at 10 °C/min under a 50 ml/min nitrogen flow rate using a sample amount of around 15 mg. All of the thermal tests were carried out in triplicate.

2.8.5. ATR-FTIR Spectroscopy

Variable-temperature Fourier transform infrared (FTIR) spectroscopy was performed using a Nicolet Nexus FTIR instrument (Thermo Fisher Scientific, Wilmington, DE) coupled to a variable-temperature single reflection diamond attenuated total reflectance (ATR) sampling accessory (Specac Ltd., Orpington, U.K.). Spectra were collected by averaging 64 scans at 4 cm^{-1} resolution using the blank ATR crystal at the same temperature as the background. The intensity of the infrared spectrum depends on a number of factors including path length and the molar extinction coefficient of the analyte. When using the ATR geometry, the path length can be considered to be constant as long as the contact between the sample and the ATR crystal is consistent. To ensure that any peak intensity changes in the data represented changes in the morphology of the samples, the samples were clamped directly onto the ATR crystal using a calibrated torque wrench (Specac Ltd., Orpington, U.K.) set at 80 cNm, which applies a load of ∼350 N via the sample accessory anvil. Reproducibility values of the sample contact and the resulting spectra intensity were validated prior to conducting the variable-temperature infrared measurements. Spectra were collected at 10 °C intervals from 30 to 100 °C and, thereafter, at 5 °C intervals up to 190 °C. To ensure validity of the selected temperature, spectra were not collected until the digital reading on the temperature controller had fully stabilized.

2.8.6. Time-Resolved Synchrotron Experiments

Simultaneous small-angle X-ray scattering (SAXS) and wide-angle X-ray scattering (WAXS) experiments as a function of temperature were carried out on beamline BL11—noncrystalline diffraction (NCD) (WAXS/SAXS station) located at the ALBA synchrotron facilities (Barcelona, Spain). The SAXS and WAXS q-axis calibrations were obtained by measuring silver behenate ($AgC_{22}H_{43}O_2$) and chromium(III) oxide (Cr_2O_3) standards, respectively. Scattering patterns were collected using the combination of two detectors, that is, a photon counting detector Pilatus 1M detector from Dectris AG (Baden, Switzerland) and a CDD WAXS LX255-HS detector from Rayonix, L.L.C. (Evanston, IL), operating simultaneously in SAXS and WAXS positions, respectively. The wavelength of the incident wave (λ) was 1 Å. The distances between the sample and the SAXS and WAXS detectors were set at 6.6328 and 0.120762 m, respectively, allowing a q-range between 0.025 and 0.22 $Å^{-1}$ for SAXS and a q-range between 0.5 and 8.4 $Å^{-1}$ for

WAXS. The beamline delivered a photon flux onto the sample of >1.5×10^{12} ph/s at 12.4 keV for a beam current of 150 mA with a bandpass ($\Delta E/E$) of 2.7×10^{-4} at 10.0 keV and a beam size at sample position of 349 μm × 379 μm. For the in situ thermal experiments, electrospun fiber mats, with a thickness of 100 μm, were placed on a "film type" THMS600 hot stage from Linkam Scientific Instruments Ltd (Epstom, U.K.). To analyze the evolution of the sample when exposed to thermal treatments, the samples were subjected to isotherms at 100 and 130 °C for up to 2 min and to thermal ramps from 0 to 180 °C at 10 °C/min.

2.8.7. Tensile Tests

The mechanical properties of the biopapers were determined in tensile conditions according to ASTM D638 using an Instron 4400 machine from Instron (Norwood, MA). Tensile tests were carried out in sextuple using 115 mm × 16 mm stamped dog-bone specimens at a cross-head speed of 10 mm/min at room temperature. The equipment was set with a load cell of 1 kN, and the specimens were preconditioned for 24 h prior to testing.

2.8.8. Permeability

The water vapor permeability (WVP) and d-limonene permeability (LP) of the biopapers were determined following the standardized gravimetric method ASTM E96-95. To do this, Payne permeability cups of 3.5 cm from Elcometer Sprl (Hermallesous-Argenteau, Belgium) were used. Both tests were performed at 25 °C in triplicate, and further details can be found elsewhere (Melendez-Rodriguez, Torres-Giner, et al. 2019).

The oxygen permeability was determined in duplicate at 60 % RH and 25 °C using an oxygen permeation analyzer M8001 (Systech Illinois, Thame, U.K.) with temperature and relative humidity control. The tested area was 5 cm^2.

2.8.9. Statistical Analysis

Analysis of variance (ANOVA) was performed using the software packaging STATGRAPHICS Centurion XVI v 16.1.03 from StatPoint Technologies, Inc. (Warrenton, VA). To evaluate the differences among the samples, Fisher's least significant difference (LSD) was set at the 95 % confidence level ($p < 0.05$).

3. Results and Discussion

3.1. Solution Properties and Morphology

The properties of the MBW-derived PHBV solution were measured and are reported in **Table 1** to evaluate its electrospinnability. One can observe that the MBW-derived PHBV solution presented a viscosity of 229.8 cP, which was significantly lower than that attained for the PHBV commercial benchmark (~689 cP), even though the concentration of the commercial biopolymer in the solution was lower. This can be related to the different solvents used for the solution as well as the higher 3HV content and potentially lower molecular weight (M_W) of the MBW-derived PHBV. In this regard, not only can the feedstock used to feed the microorganisms affect the M_W of the resultant PHA but also the chemical digestion methods that were applied to disrupt the cell wall and then release PHAs (Kunasundari and Sudesh 2011). In any case, the attained value of viscosity is appropriate for electrospinning since it was similar to that reported for solutions containing 2 wt % PHBV obtained from fruit pulp biowaste purified using chloroform, that is, 296.8 cP (Melendez-Rodriguez et al. 2018). In the case of surface tension and conductivity, the MBW-derived PHBV solution presented values of 26.2 mN/m and 0.14 μS/cm, respectively. The surface tension was very similar for both PHBV solutions and also comparable to other PHAs derived from biowaste, which were reported in the 20.5–21.9 mN/m range, but the conductivity was lower, that is, 1.3–3.7 μS/cm range (Melendez-Rodriguez et al. 2018). The latter value can be ascribed to the low amount of remaining conductive impurities, and it represents a positive indicator for electrospinning since polymer solutions with high conductivities usually show lower processability (Torres-Giner et al. 2017).

Table 1. Properties of commercial and municipal biowaste (MBW)-derived poly(3-hydroxybutyrate-*co*-3-hydroxyvalerate) (PHBV) solutions.

Sample	Concentration (wt %)	Viscosity (cP)	Surface tension (mN/m)	Conductivity (μS/cm)
Commercial PHBV	10	688.8 ± 2.3[a]	21.9 ± 0.1[a]	3.74 ± 0.02[a]
MBW-derived PHBV	15	229.8 ± 1.5[a]	26.2 ± 0.3[a]	0.14 ± 0.01[a]

[a] Different letters in the same column mean a significant difference among the samples ($p < 0.05$).

Figure 1 shows the mats obtained after the electrospinning process of the MBW-derived PHBV solutions, before and after annealing, both the cryo-fracture surfaces and the top views. One can observe in the figure at room temperature, which corresponds to the electrospun mat without thermal post-treatment, that electrospinning yielded a mat composed of nonwoven ultrathin fibers. For instance, the electrospinning of the PHBV solution yielded homogenous and bead-free fibers having a mean diameter of 1.12 ± 0.12 μm. It can also be noticed that the application of annealing temperatures of 80, 110, and 125 °C resulted in a rearrangement of the fine fibers, but the material still maintained a high porosity level. At 130 °C, interestingly, the electrospun PHBV mat turned into a continuous film with a very low porosity due to the fiber coalescence process.

This phenomenon is due to the compact packing rearrangement of the electrospun fibers to reduce their surface energy at temperatures below the biopolymer's T_m (Cherpinski et al. 2017). **Figure 2** displays, as an example, a zoomed top view of the biopaper annealed at 130 °C, which proved that the material is constituted by aligned side-by-side fibers of approximately 1.2–2 μm with minimal porosity.

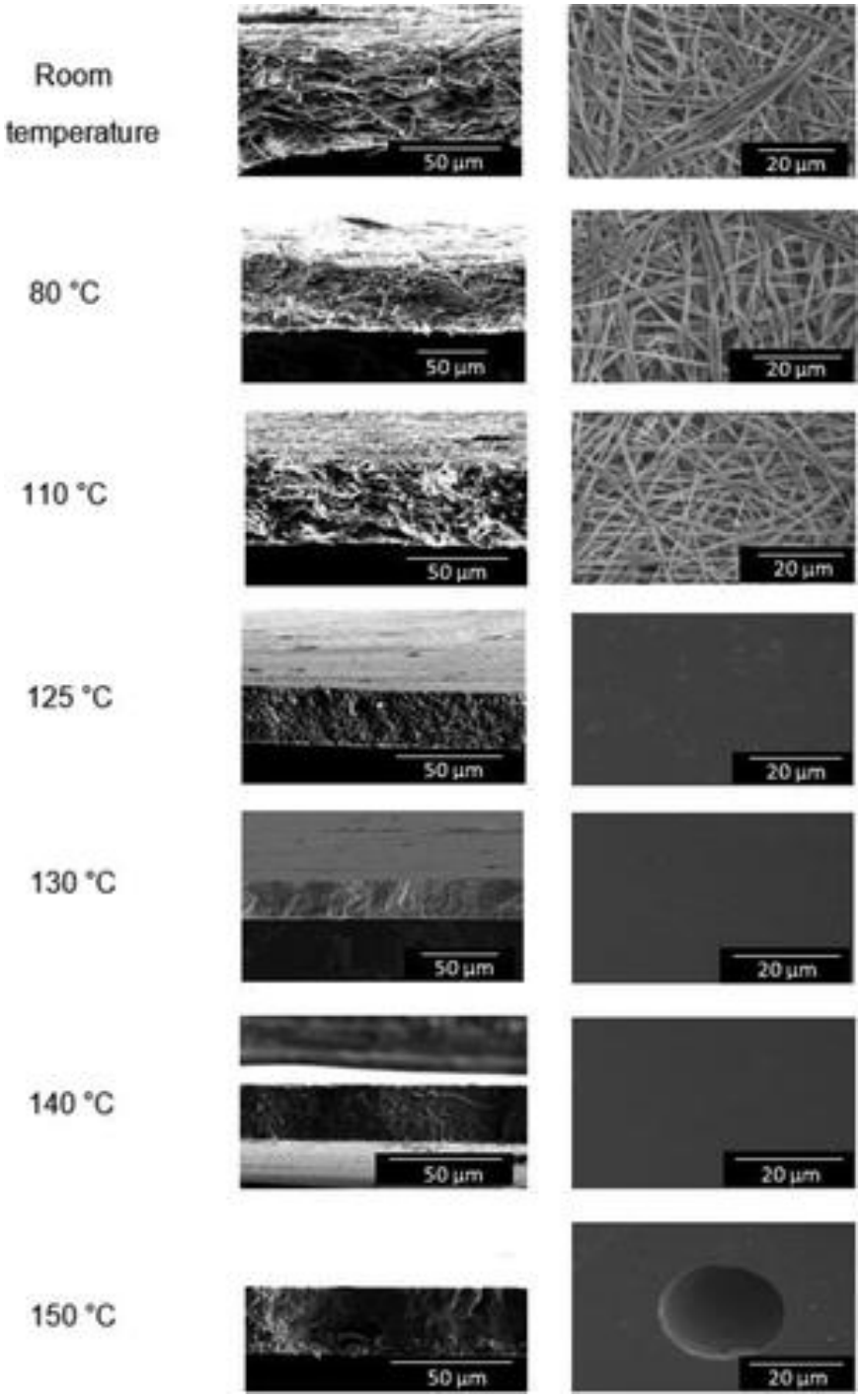

Figure 1. SEM images of the cross section (left) and top view (right) of the electrospun MBW-derived PHBV mats without thermal post-treatment and annealed at 80, 110, 125, 130, 140, and 150 °C for 5 s. Scale markers are of 50 and 20 μm, respectively.

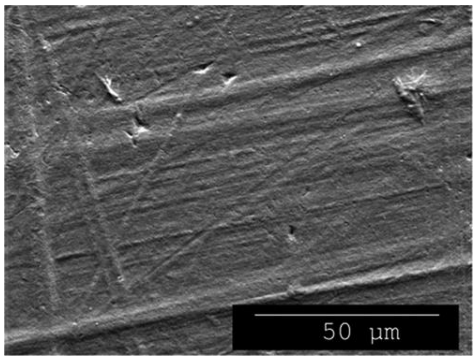

Figure 2. SEM image of the top view of the electrospun MBW-derived PHBV mat annealed at 130 °C for 5 s. Scale marker is of 50 µm.

Figure 1 also shows that at higher temperatures, that is, at 150 °C, some large voided areas were formed, which could be the result of thermal deterioration and release of volatile components. A similar film morphology evolution was recently observed for electrospun fiber mats of fruit-residue-derived PHBV (Melendez-Rodriguez et al. 2018). Based on the morphology observations, the electrospun mats postprocessed at 130 °C were selected for further characterization.

3.2. Optical Properties

Figure 3 displays the background transparency pictures of resulting annealed electrospun mats of MBW-derived and commercial PHBV. It can be observed that both biopapers show certain transparency and lack of color, suggesting that the PHBVs presented low crystallinity and were not thermally abused, respectively. Electrospinning is known to result in low-crystallinity materials due to the very rapid solidification process of the polymer jet. In the case of the MBW-derived PHBV, the samples showed even higher transparency associated with the higher 3HV content, which is known to yield materials with lower melting point, crystallinity, and density.

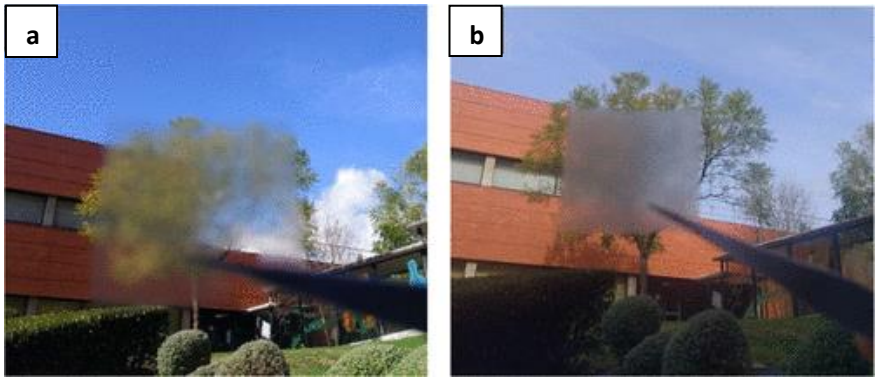

Figure 3. Background transparency pictures of the electrospun PHBV biopapers: (a) derived from MBW and (b) commercial grade.

To quantify the color properties of the electrospun biopaper of PHBV, the lightness and color parameters were determined by the values of L^* and a^* b^* coordinates, respectively. One can observe in **Table 2** that the MBW-derived PHBV biopaper showed a value of L^* of 89.39, while the values of a^* and b^* were −0.2 and 2.13, indicating that it was relatively luminous and only slightly yellow. These values were very similar to those obtained for the electrospun films of PHBV derived from fruit pulp biowastes, though the present samples showed slightly higher values of a^* and b^* (Figueroa-Lopez et al. 2019). Interestingly, the electrospun biopapers were brighter than PHB/PHBV blend films obtained by melt processing routes, which showed a value of L^* of 86.40 (Melendez-Rodriguez, Torres-Giner, et al. 2019). In terms of color difference, the electrospun biopaper made of MBW-derived PHBV showed a color difference of 1.03, which is nearly unnoticeable ($\Delta E^* < 1$) and it can be noticed only by an experienced observer ($\Delta E^* \geq 1$ and < 2). Regarding transparency and opacity, one can also observe that the MBW-derived PHBV biopaper presented a higher value of T and lower value of O than the biopaper made of commercial PHBV, which means that the biopaper obtained from MBW was more transparent and developed a less grayish color than the commercial one. This optical property can be regarded as an advantage for food packaging because transparency is associated with conventional plastics used in packaging and is better accepted by users. In this regard, Jung et al. (Jung et al. 2020) induced a color change from yellowish to bluish in PHB films to make them more commercially attractive.

Table 2. Optical properties of the electrospun PHBV biopapers.

Film	a^*	b^*	L^*	ΔE^*	T	O
Commercial PHBV	0.35 ± 0.03^a	1.29 ± 0.01^a	89.14 ± 0.02^a	-	9.20 ± 0.08^a	0.07 ± 0.02^a
MBW-derived PHBV	-0.20 ± 0.02^a	2.13 ± 0.03^a	89.39 ± 0.03^a	1.03 ± 0.02	2.56 ± 0.02^a	0.010 ± 0.001^a

[a] Different letters in the same column mean significant difference among the samples ($p < 0.05$).

3.3. Thermal Properties

Thermal characterization was measured on the selected MBW material annealed at 130 °C, since the full physicochemical characterization of the electrospun commercial PHBV material was published elsewhere (Melendez-Rodriguez, Figueroa-Lopez, et al. 2019). The DSC data for the other samples processed at the different temperatures are gathered in **Table S1**, which is included in the Supporting Information. The DSC curves, corresponding to the heating and cooling steps, of the MBW-derived PHBV biopaper, are presented in **Figure 4**. **Table 3** summarizes the main thermal values obtained from the DSC curves for the MBW-derived PHBV, and the values of the commercial PHBV were also included for comparison purposes. During the first heating, the sample showed a broad single melting endotherm at 154 °C with a shoulder at lower temperatures and with ΔH_m of nearly 58 J/g. In the cooling step, one can notice that the biopolymer crystallized from the melt in a broad range, showing a dominant peak corresponding to the crystallization temperature from the melt (T_c) at 60.3 °C and an enthalpy of crystallization (ΔH_c) of 38.1 J/g. Moreover, during the second heating step, the MBW-derived PHBV material further cold-crystallized and it showed a cold crystallization temperature (T_{cc}) at approximately 45 °C with an enthalpy of cold crystallization (ΔH_{cc}) of 9.8 J/g. The glass-transition temperature (T_g) of the

biopolymer was noticeable at −5 °C during the second heating. Moreover, the sample showed two endothermic melting peaks. The first one was observed at 132.4 °C, followed by a more intense second one at 149.4 °C, with a total enthalpy of melting (ΔH_m) of 60.5 J/g. A similar thermal behavior was observed previously for PHBV obtained from pulp fruit biowaste having a higher 3HV content, that is, approximately 20 mol % (Melendez-Rodriguez et al. 2018). Cold crystallization was unnoticeable in the complex melting endotherms, but this process cannot be ruled out. The presence of multiple melting peaks in a relatively low thermal range is linked to a dynamic crystal reorganization upon heating, where imperfect crystals develop thicker lamellar thicknesses during heating and thereafter melt at higher temperatures. This phenomenon, supported here by the below synchrotron and ATR-FTIR experiments, was previously observed and discussed by, among others, Zhang et al. (Zhang, Misra, and Mohanty 2014) in PHA copolyesters. The commercial biopaper, however, showed a single melting endotherm in the 170–172 °C range, both in the first heating and in the second one, with a T_c value at approximately 117 °C (Melendez-Rodriguez, Figueroa-Lopez, et al. 2019). These differences among both PHBV samples can be mainly ascribed to the different 3HV contents. In comparison with other PHBV films with different 3HV contents, Sanchez-Garcia et al. (Sanchez-Garcia, Gimenez, and Lagaron 2008) showed that copolyesters with 12 mol % 3HV exhibited double melting with peaks centered at approximately 145 and 157 °C. Elsewhere, Castro-Mayorga et al. (Castro Mayorga et al. 2018) showed that PHBV blends with contents of 3 and 18 mol % 3HVs also presented double-melting peaks with T_m values of 169.6 and 173.2 °C. In the case of the homopolyester, PHB showed only one melting peak at 169.4 °C (Cherpinski et al. 2017). Due to their higher 3HV contents, the T_m values of the MBW-derived PHBV were lower than the PHB ones and slightly higher than those obtained for PHBV derived from fruit pulp biowaste with 20 mol % 3HV, with a single melting peak at 139 °C (Melendez-Rodriguez et al. 2018). In the above works by the authors, the inherently complex thermal behavior generated during the dynamic DSC runs is highlighted as well as the difficulties in establishing reliable crystallinity data. It should be noted that many of these copolymers recently synthesized have never been studied in sufficient detail to determine, for instance, the enthalpy of melting for an infinity crystal (ΔH_m^0), required for crystallinity determination.

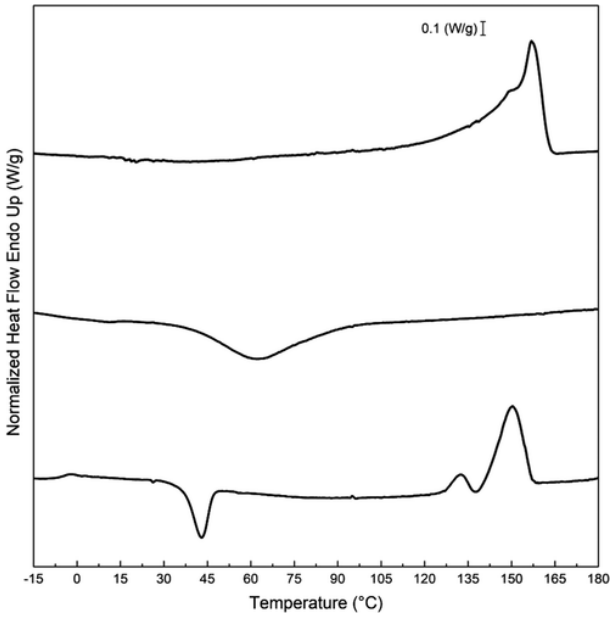

Figure 4. DSC curves taken, from top to bottom, during the first heating, cooling, and second heating of the electrospun biopaper of PHBV derived from MBW.

Table 3. Thermal properties of the electrospun PHBV biopapers obtained by DSC and TGA.

Biopaper	DSC									TGA			
	First heating		Cooling		Second heating								
	T_m (°C)	ΔH_m (J/g)	T_c (°C)	ΔH_c (J/g)	T_g (°C)	T_{cc} (°C)	ΔH_{cc} (J/g)	T_m (°C)	ΔH_m (J/g)	$T_{5\%}$ (°C)	T_{deg} (°C)	Mass loss at T_{deg} (%)	Residual mass (%)
Commercial PHBV*	171.5 ± 0.4[a]	75.2 ± 0.6[a]	116.8 ± 0.5[a]	85.6 ± 0.2[a]	2.6 ± 0.4[a]	-	-	170.4 ± 0.2[a]	83.2 ± 3.0[a]	259.9 ± 1.2[a]	277.3 ± 0.6[a]	62.0 ± 0.8[a]	2.0 ± 0.2[a]
MBW-derived PHBV	153.9 ± 0.1[b]	57.4 ± 5.4[b]	60.3 ± 1.9[b]	38.1 ± 5.5[b]	–5.0 ± 1.2[b]	44.7 ± 0.3[b]	9.8 ± 4.1[b]	132.4 ± 0.7[b] // 149.4 ± 0.3[c]	60.5 ± 0.6[b]	204.7 ± 2.0[b]	239.9 ± 0.8[b]	94.8 ± 1.7[b]	0.2 ± 0.1[b]

* Data reported in a previous study (Melendez-Rodriguez, Figueroa-Lopez, et al. 2019).

[a-c] Different letters in the same column mean significant difference among the samples ($p < 0.05$).

In **Table 3**, the thermal stability values of the MBW-derived PHBV and commercial biopapers obtained from TGA were also included. It can be observed that the copolyester presented a temperature at 5 % weight loss ($T_{5\%}$), considered as the onset-degradation temperature (T_{onset}), of ~205 °C. Its thermal degradation temperature (T_{deg}) occurred at ~240 °C, associating a mass loss of nearly 95 %, whereas the amount of residual mass was 0.2 %. Previously prepared films of PHBV with a 3HV content of 18 mol % were also thermally stable up to 249.8 °C (Castro-Mayorga, Fabra, and Lagaron 2016). However, other studies reported that PHBV with different 3HV contents showed higher thermal stability. For instance, PHBV with 20 mol % 3HV showed $T_{5\%}$ and T_{deg} values of approximately 267 and 290 °C, respectively, (Melendez-Rodriguez et al. 2018) while commercial PHBV with a 3HV content of 3 mol % showed $T_{5\%}$ and T_{deg} values of approximately 260 and 277 °C, respectively (Melendez-Rodriguez, Figueroa-Lopez, et al. 2019). This observation points out that thermal stability was not only dependent on the 3HV content but also related to other factors such as M_W, purity, or the presence of additives. Finally, it is also worthy to mention that a residue of 0.2 % was attained at 800 °C, which indicates that the extraction and purification process successfully removed any potential inorganic residues from the feedstock.

3.4. Crystalline Morphology

Figure 5 shows the evolution of the ATR-FTIR spectra of the electrospun fibers up 200 °C to determine the changes with heating of the molecular order of the MBW-derived PHBV. Moreover, in **Figure 6**, the evolution of the ratio of the absorbance of the bands 1230/1453 and the 1720 cm^{-1} full width at half-height-maximum (FWHH) for the MBW-derived PHBV fibers obtained by electrospinning are represented as a function of temperature. These two spectral features are related to the molecular order (crystallinity) in the biopolymer (Cherpinski et al. 2017). In particular, for PHA copolyesters, the stretching vibration of the carbonyl group ν(C═O) corresponds to the strongest peak observed at 1720 cm^{-1}. Furthermore, the complex and multiple peaks that were visible from 1000 to 880 cm^{-1} are known to arise from the stretching bands of the

carbon–carbon single bond ν(C–C) (Torres-Giner et al. 2016). Finally, the band centered at ~1080 cm^{-1} was related to ester bonds in the biopolymer, whereas the band at ~1020 cm^{-1} corresponding to C–O and C–O–C has been ascribed to stretching vibrations of ester groups in biopolyesters (Torres-Giner et al. 2011). Thus, both higher 1230/1453 bands ratios and lower 1720 cm^{-1} band widths were correlated previously with higher crystallinity in the biopolymer (Cherpinski et al. 2017).

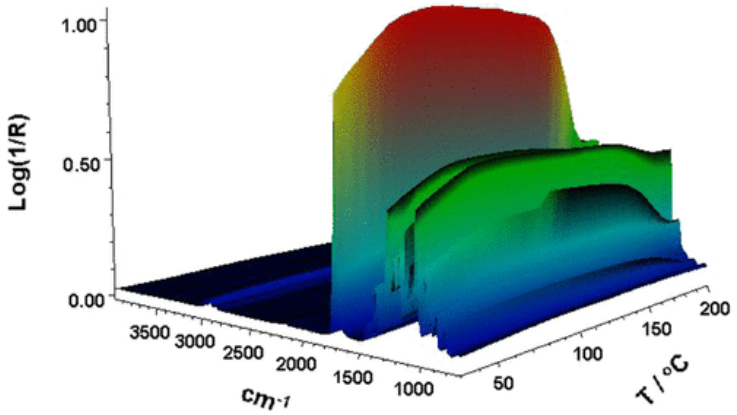

Figure 5. ATR-FTIR spectra taken across temperature of the electrospun MBW-derived PHBV fibers.

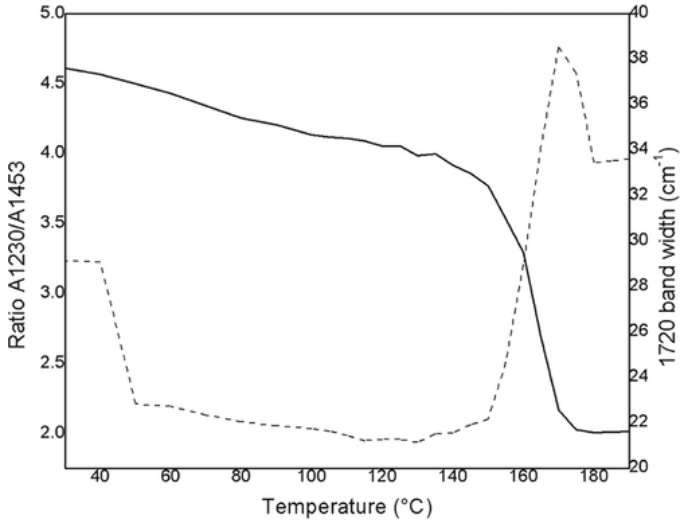

Figure 6. Evolution as a function of temperature of the ratio of the absorbance of the bands 1230/1453 (continuous line) and the 1720 cm^{-1} band full width at half-height-maximum (dashed line) for the electrospun MBW-derived PHBV fibers.

In the ATR-FTIR spectra, it was observed that with increasing temperature the electrospun material exhibited a continuous rise in intensity of the carbonyl band, seen at 1720 cm^{-1}, among

other peaks, up to approximately 130 °C. The band intensity started to decrease at temperatures higher than 130 °C. Moreover, the peak concomitantly increased its width and shifted toward higher wavenumbers. From this, one can infer that the molecular order initially increased with temperature up to about 130 °C, and after 140 °C, it sharply decreased prior to melting. This annealing phenomenon was however not picked up by the 1230/1453 band ratio, which decreased monotonically with increasing temperature, being more pronounced in the vicinity of melting, after 140 °C. These results, but specifically the ∼1720 cm^{-1} band evolution, do shed some light on the process of fiber coalescence observed by SEM, suggesting that this process takes place below the biopolymer melting point and is connected with a sufficiently thermally induced improvement in the molecular order and the presumed mobility of the fibers during that process to reduce surface tension.

The crystallinity and phase morphology of the electrospun MBW-derived PHBV fibers were further assessed by simultaneous time-resolved SAXS and WAXD experiments as a function of temperature using synchrotron radiation. These X-ray diffraction techniques are very useful to assess crystallinity, crystalline morphology, and the phase structure at the mesoscale in semicrystalline biopolymers (Riekel et al. 2003). **Figure 7** displays the simultaneous SAXS and WAXD diffractograms of the electrospun fibers in both isotherm conditions at 100 and 130 °C and for a thermal ramp from 0 to 180 °C at 10 °C/min (analogous to the DSC conditions). In the case of the isotherm at 130 °C, which intends to follow in situ the phase morphology alterations occurring in the sample during the annealing process, the SAXS diffractograms indicate that the peak associated with the long period (Sato et al. 2012) becomes better resolved after a few seconds at this temperature, again supporting the FTIR observations of the improved molecular order and phase structure regularity, developing during the annealing process. During the thermal ramp to melting, the SAXS peak became stronger with increasing temperature with the maximum at approximately 130 °C and after the peak begins to shift toward lower q values, implying an increase in the long period associated with longer repeat units prior to melting. **Figure 7** also shows the WAXD diffractogram evolution over time, exhibiting the most characteristic peaks of the PHB crystal at 2θ 8.8 and 11°, which correspond to the (020) and (110) diffractions, respectively, that arise from the lattice planes of the orthorhombic unit cells (Sato et al. 2012). The WASX diffractograms also exhibited four minor reflections at approximately 13.5, 16, 17.1, and 22°, which originate from the (021), (111), (121), and (040) lattice planes (Panaitescu et al. 2017, Vahabi et al. 2019). According to the literature, the PHB crystal lattice is representative of PHBV copolyesters based on up to 37 mol % 3HV (Škrbić and Divjaković 1996). **Figure 8** zooms the evolution of the peak corresponding to the (110) plane for the isotherms and for the heating ramp. In the case of the isotherms, it can be clearly observed that the crystalline peak increases in relative intensity with time, especially at 130 °C, suggesting again that the crystallinity and crystalline morphology improved during the first 20 s of the isothermal treatment.

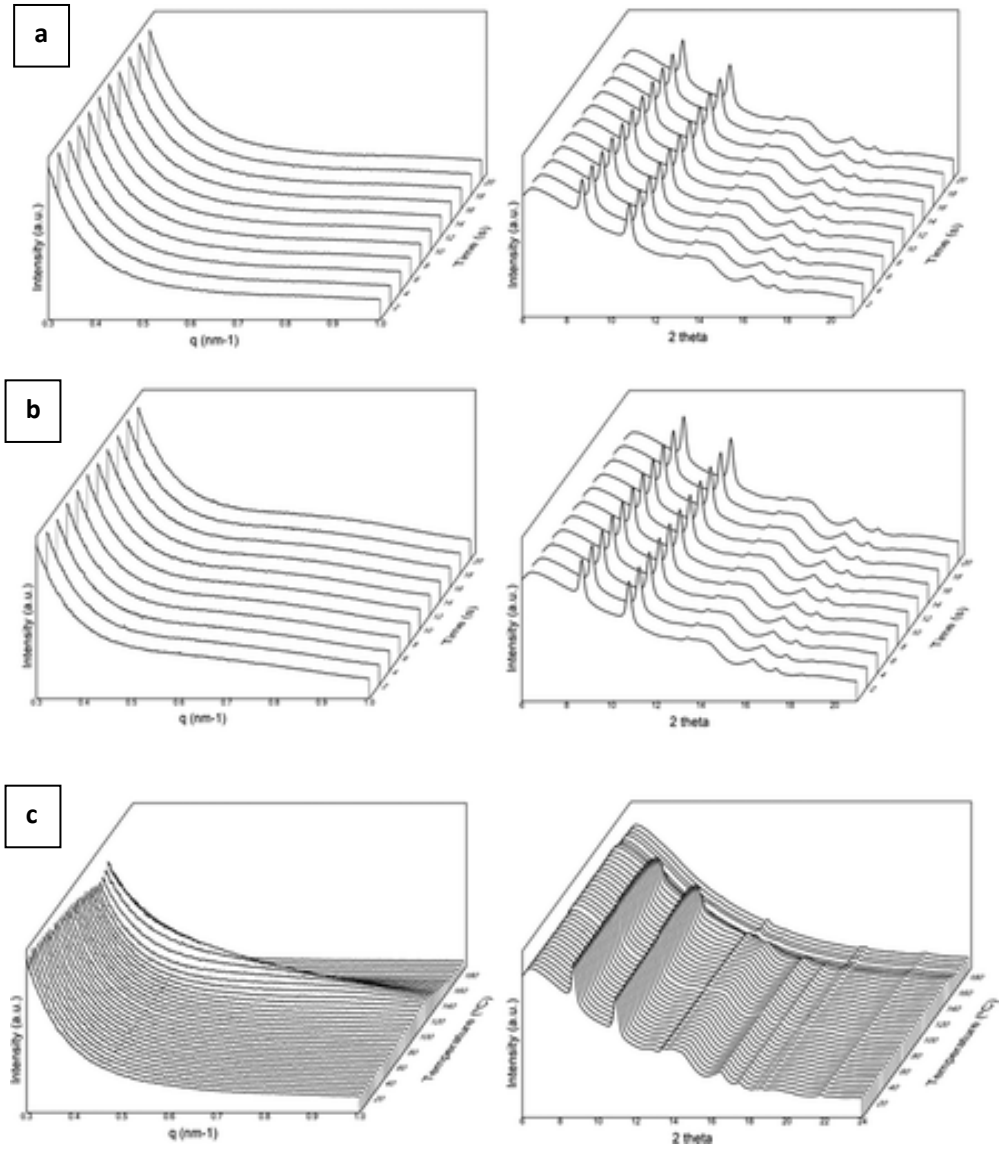

Figure 7. SAXS (left) and WAXS (right) pattern evolution of the electrospun MBW-derived PHBV fibers at (a) 100 °C for 20 s; (b) 130 °C for 20 s; and (c) during a thermal ramp from 0 up to 180 °C at 10 °C/min.

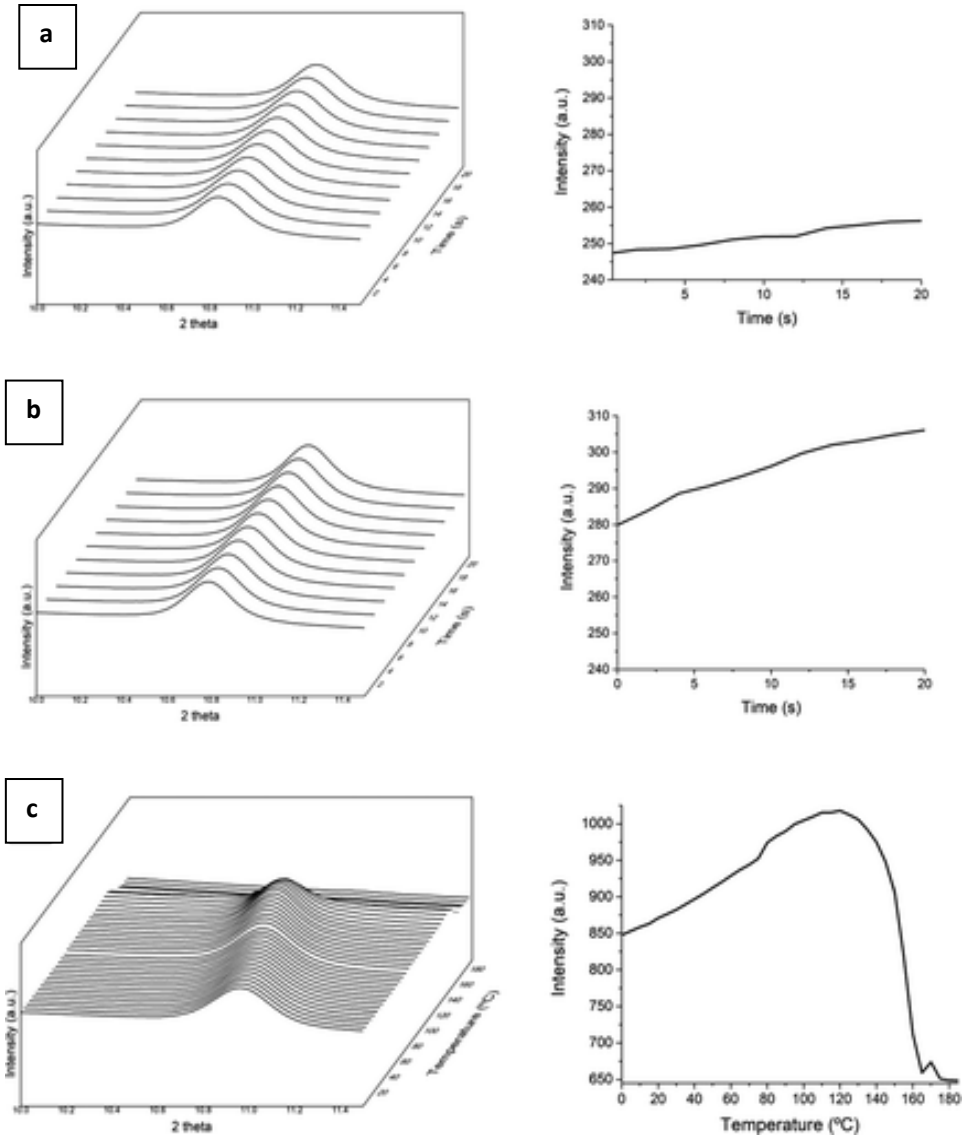

Figure 8. WAXS patterns zoomed around the 2θ 11° peak of the electrospun MBW-derived PHBV fibers for the two isotherms (a, b) and heating ramp (c) in **Figure 7**. The right plots quantify the evolution in relative intensity of the 2θ 11° peak seen in the left diffractograms.

From the heating ramp in **Figure 7** and **8**, it was also observed that the WAXD patterns, in good agreement with the SAXS pattern behavior, underwent a relative intensity increase, suggesting a clear improvement in phase morphology and crystallinity with increasing temperature up to 130 °C, followed by a sharp decrease associated with melting beyond 150 °C, which again correlates very well with the changes observed from FTIR spectroscopy in **Figure 6**.

3.5. Mechanical Performance

Figure 9 displays the stress vs strain curve of the MBW-derived PHBV biopaper. From this curve, the main mechanical properties were obtained and are summarized in **Table 4**. This table indicates that the biopaper presents characteristic properties of a rigid and brittle material, in good resemblance with some of the best commercial papers (Harini and Sukumar 2019, Tanpichai et al. 2020). In particular, the mean values of elastic modulus (E) and tensile strength at yield (σ_y) were 1583 and 13.6 MPa, respectively, whereas the elongation at break (ε_b) and toughness (T) values were below 3 % and 0.5 mJ/m^3, respectively. For the commercial PHBV biopaper, the values obtained were in the same range as the MBW-derived PHBV biopaper, which presented values of 1252 and 18.1 MPa for E and σ_y, respectively, whereas ε_b was 2.4 % and T was 0.3 mJ/m^3 (Melendez-Rodriguez, Figueroa-Lopez, et al. 2019). In comparison with other electrospun PHA films, the mechanical properties of the here-obtained MBW-derived PHBV are closer than those found by Cherpinski et al. (Cherpinski, Torres-Giner, Vartiainen, et al. 2018) who reported E and σ_y values in the range of 1000–2000 and 14–28 MPa, respectively, and an ε_b value of approximately 3 % for PHB and PHBV films prepared by electrospinning. Moreover, our recent studies also showed similar mechanical values for electrospun films of PHBV derived from fruit pulp biowaste in which the mean values of E, σ_y, and ε_b were 1200 MPa, 18 MPa, and 2.5 %, respectively (Melendez-Rodriguez et al. 2018). Furthermore, when compared with PHBV films prepared by compression molding, the here-developed biopapers showed higher ductility and toughness and slightly lower mechanical strength (Shibata et al. 2004, Torres-Giner, Hilliou, et al. 2018). These differences have been ascribed to both the inherently lower crystallinity generated by the electrospinning process and the particular biopaper morphology being constituted by an assembly of nonmolten ultrathin fibers (Cherpinski et al. 2017). In this regard, Alp-Erbay et al. (Alp-Erbay et al. 2019) also indicated that the interactions between the coalesced electrospun fibers (e.g., point bonding, slip of fibers over one another, alignment, among other phenomena) were responsible for the somewhat higher mechanical flexibility attained in the annealed electrospun materials.

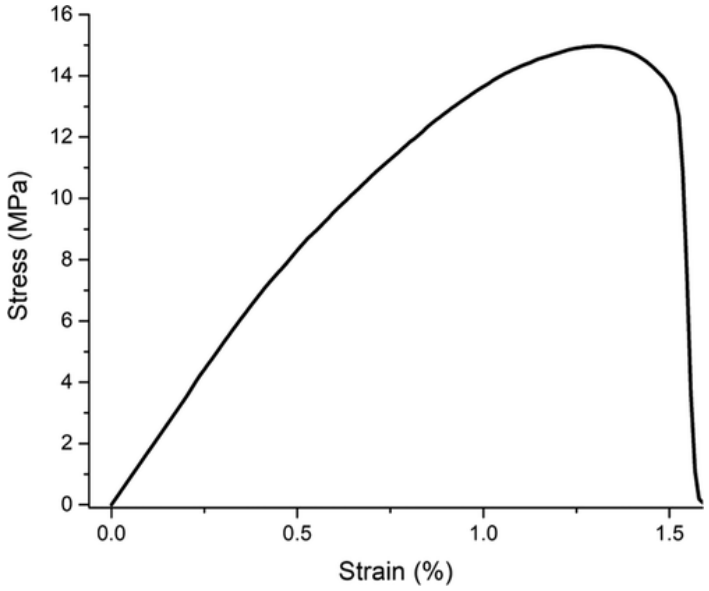

Figure 9. Typical tensile stress–strain curve of the electrospun MBW-derived PHBV biopaper.

Table 4. Mechanical properties of the electrospun PHBV biopapers.

Biopaper	E (MPa)	σ_y (MPa)	ε_b (%)	T (mJ/m^3)
Commercial PHBV*	1252 ± 79[a]	18.1 ± 2.1[a]	2.4 ± 0.3[a]	0.3 ± 0.1[a]
MBW-derived PHBV	1583 ± 249[a]	13.6 ± 3.3[a]	1.3 ± 0.4[b]	0.10 ± 0.01[a]

* Data reported in a previous study (Melendez-Rodriguez, Figueroa-Lopez, et al. 2019).

[a-b] Different letters in the same column mean significant difference among the samples ($p < 0.05$).

In a sustainable packaging context application, the mechanical properties of the MBW-derived PHBV biopaper are similar in terms of mechanical strength but somewhat less ductile than thermo-compressed films of polylactide (PLA), which showed E, σ_y, and ε_b values of 822.5 MPa, 39.6 MPa, and 5.5 %, respectively (Quiles-Carrillo et al. 2019b). In comparison with currently used petroleum-derived polymers, PET films show values of E, maximum tensile strength (σ_{max}), and ε_b in the ranges of 1000–1100 MPa, 50–60 MPa, and 50–90 %, respectively (Thomas and Visakh 2011). In the case of LDPE, its films are remarkably more flexible and ductile (Ali Dadfar et al. 2011). Therefore, the MBW-derived PHBV biopaper showed high rigidity and mechanical strength but a somewhat brittle behavior that is further supported by the lack of yielding in the tensile stress vs strain curve. However, if a comparison is drawn with conventional papers, these materials show lower resistance but somewhat higher ductility and flexibility, having E, σ_y, and ε_b values in the ranges of 500–700 MPa, 60–70 MPa, and 10–12 %, respectively (Harini and Sukumar 2019, Tanpichai et al. 2020).

3.6. Barrier Properties

The WVP, LP, and OP values of the electrospun MBW-derived PHBV biopaper are shown in **Table 5**. It can be observed that the here-produced biopaper presented a WVP value of 3.99×10^{-14} $kg \cdot m \cdot m^{-2} \cdot Pa^{-1} \cdot s^{-1}$, while its LP was 2.09×10^{-14} $kg \cdot m \cdot m^{-2} \cdot Pa^{-1} \cdot s^{-1}$. These values are clearly superior to uncoated conventional papers (Hu et al. 2018) and quite similar to but slightly lower than those obtained for the commercial PHBV biopaper, which showed WVP and LP values of 5.34×10^{-14} and 2.68×10^{-14} $kg \cdot m \cdot m^{-2} \cdot Pa^{-1} \cdot s^{-1}$, respectively (Melendez-Rodriguez, Figueroa-Lopez, et al. 2019). In comparison with other PHA films reported in the literature, the values obtained herein are higher than those reported for electrospun PHB films, that is, 5.22×10^{-15} and 3.20×10^{-15} $kg \cdot m \cdot m^{-2} \cdot Pa^{-1} \cdot s^{-1}$ for WVP and LP, respectively (Cherpinski et al. 2017). This barrier reduction is related to the lower crystallinity content developed in the copolyester, indicating as expected that the barrier properties decrease on increasing the 3HV content (Sanchez-Garcia, Gimenez, and Lagaron 2008). When compared with other PHBV films, the permeability of the here-prepared biopaper is in the same range. Thus, for PHBV with 3 mol % 3HV, the values obtained were 5.3×10^{-14} and 2.7×10^{-14} $kg \cdot m \cdot m^{-2} \cdot Pa^{-1} \cdot s^{-1}$ for WVP and LP, respectively (Melendez-Rodriguez, Torres-Giner, et al. 2019). For PHBV with a higher 3HV content, that is, 20 mol % 3HV, the values were in the range of $(1–3) \times 10^{-14}$ $kg \cdot m \cdot m^{-2} \cdot Pa^{-1} \cdot s^{-1}$ for WVP and $(0.3–3.5) \times 10^{-14}$ $kg \cdot m \cdot m^{-2} \cdot Pa^{-1} \cdot s^{-1}$ for LP (Melendez-Rodriguez et al. 2018). In relation to PHA films prepared by other techniques, solvent-cast PHBV films showed a slightly

higher barrier to limonene and water vapors. In particular, the WVP was 1.27×10^{-14} kg·m·m^{-2}·Pa^{-1}·s^{-1} and the LP was 1.99×10^{-13} kg·m·m^{-2}·Pa^{-1}·s^{-1} for films made of PHBV containing 3 mol % 3HV (Sanchez-Garcia, Gimenez, and Lagaron 2008). Similarly, compression-molded PHB films showed a WVP of 1.7×10^{-15} kg·m·m^{-2}·Pa^{-1}·s^{-1} and an LP value of 8.8×10^{-15} kg·m·m^{-2}·Pa^{-1}·s^{-1} (Sanchez-Garcia, Gimenez, and Lagaron 2007). The slightly lower barrier performance attained for the electrospun biopaper is ascribed to the particular fiber alignment, still leaving some porosity due to its fibrillar nature.

Table 5. Permeability of the electrospun PHBV biopapers.

Biopaper	**WVP × 10^{14} (kg·m·m^{-2}·Pa^{-1}·s^{-1})**	**LP × 10^{14} (kg·m·m^{-2}·Pa^{-1}·s^{-1})**	**OP × 10^{20} (m^3·m·m^{-2}·Pa^{-1}·s^{-1})**
Commercial PHBV*	5.34 ± 1.79[a]	2.68 ± 1.82[a]	3.74 ± 0.6[a]
MBW-derived PHBV	3.99 ± 1.32[a]	2.09 ± 0.30[a]	2.88 ± 0.36[a]

* Barrier data reported in a previous study (Melendez-Rodriguez, Figueroa-Lopez, et al. 2019).

[a] Different letters in the same column mean significant difference among the samples ($p < 0.05$).

The electrospun MBW-derived PHBV biopapers also presented good barrier properties to oxygen. In particular, the OP value was 2.88×10^{-20} m^3·m·m^{-2}·Pa^{-1}·s^{-1}, which is in the range of other electrospun PHA films, such as PHBV with 3 mol % 3HV (3.74×10^{-20} m^3·m·m^{-2}·Pa^{-1}·s^{-1}) (Melendez-Rodriguez, Figueroa-Lopez, et al. 2019), PHBV with 20 mol % 3HV (1.25×10^{-19} m^3·m·m^{-2}·Pa^{-1}·s^{-1}) (Melendez-Rodriguez et al. 2018), and PHB (1.20×10^{-18} m^3·m·m^{-2}·Pa^{-1}·s^{-1}) (Cherpinski, Torres-Giner, Vartiainen, et al. 2018). Since oxygen is more sensitive to the material free volume, morphological differences, and defects than vapors of higher M_W, the measured value indicates that the here-attained electrospun biopaper of PHBV derived from MBW presents a good uniformity and reduced porosity. In the context of packaging applications, the OP value obtained here is lower than in PET films (1.35×10^{-19} m^3·m·m^{-2}·Pa^{-1}·s^{-1}) but is considerably lower in comparison with that of LDPE films (2.15×10^{-17} m^3·m·m^{-2}·Pa^{-1}·s^{-1}). On the other hand, the permeability to oxygen is higher than that of a high-barrier ethylene–vinyl alcohol copolymer (EVOH) (7.7×10^{-20} m^3·m·m^{-2}·Pa^{-1}·s^{-1}) (Lagarón 2011).

4. Conclusions

In the present study, a PHBV material derived from municipal biowaste was developed, purified, ran by electrospinning, and postprocessed by a mild thermal treatment at 130 °C for 5 s, to obtain a fiber-based continuous film: the so-called biopaper. The resultant fiber-based film exhibited higher transparency and a less grayish color than a commercial PHBV. The thermal properties exhibited a multiple melting endotherm with the maximum of melting at approximately 155 °C. The material remained stable up to ∼205 °C, and the maximum of degradation occurred at approximately 240 °C. Interestingly, molecular order, crystallinity, and phase morphology at the mesoscale were assessed by ATR-FTIR spectroscopy and time-resolved simultaneous WAXS and SAXS experiments using synchrotron radiation as a function of temperature and were found to correlate very well with each other. The results indicated that by heating the electrospun fibers up until 130 °C, the phase morphology and crystallinity are improved; beyond this temperature, the crystallinity begins to deteriorate until complete melting occurs. This improvement in phase morphology upon heating, resulting from thermally activated molecular chain rearrangements, allows the fibers to coalesce to reduce surface tension and hence to reduce structural porosity. In terms of mechanical properties, the biopaper was found to exhibit higher mechanical strength but somewhat lower ductility than commercial papers. However, the biopapers showed higher ductility and toughness than similar PHBV films prepared by melt compounding routes. These differences were ascribed to the particular morphology of the electrospun biopaper, having ill-defined crystallinity and being composed of aligned side-by-side fibers. Finally, in terms of barrier properties, the biopaper is clearly superior to traditional cellulose papers and showed similar values to other electrospun PHA films being slightly more permeable than their compression-molded counterpart films. In any case, the film showed high barrier to water vapor and oxygen and, hence, great interest in food packaging applications.

From the evidence presented, it can be concluded that the use of MBW is of significant interest to develop more sustainable packaging materials from both an environmental and an economic point of view, in full alignment with circular bioeconomy strategies, since the production of PHAs by these mixed microbial cultures can successfully minimize the costs associated with the fermentation and downstream processes. Furthermore, the combination of electrospinning and a mild annealing postprocessing below the biopolymer's T_m is able to yield unique biomaterials with balanced properties.

5. Supporting Information

Table S1. Thermal properties of the electrospun biopapers of MBW derived PHBV annealed at different temperatures and obtained from the first heating, subsequent cooling, and second heating runs by DSC.

Biopaper	DSC							
	First heating		Cooling		Second heating			
	T_m (°C)	ΔH_m (J/g)	T_c (°C)	ΔH_c (J/g)	T_{cc} (°C)	ΔH_{cc} (J/g)	T_m (°C)	ΔH_m (J/g)
As obtained	155.4 ± 1.5^{a,b}	57.6 ± 2.2^{a,c}	68.1 ± 4.1^{a}	43.9 ± 8.2^{a}	44.9 ± 0.7^{a}	4.6 ± 0.4^{a}	136.0 ± 2.8^{a} // 152.4 ± 2.5^{a}	56.7 ± 1.6^{a}
80 ºC	156.9 ± 1.9^{a}	61.7 ± 4.2^{a,b}	60.1 ± 2.1^{b}	42.3 ± 1.7^{a}	37.9 ± 1.3^{b}	3.7 ± 0.6^{a}	135.8 ± 4.4^{a,b} // 151.7 ± 2.3^{a}	62.9 ± 4.2^{b}
110 ºC	156.5 ± 2.6^{a}	62.2 ± 0.9^{b}	59.8 ± 2.5^{b}	37.5 ± 3.5^{a}	44.8 ± 0.6^{a}	9.5 ± 2.6^{b}	132.1 ± 0.5^{b} // 149.7 ± 0.6^{a}	63.6 ± 1.0^{b}
125 ºC	153.6 ± 0.7^{b}	56.2 ± 4.3^{a,c}	59.8 ± 1.7^{b}	38.5 ± 2.6^{a}	45.4 ± 1.1^{a}	5.1 ± 2.4^{a,b}	131.8 ± 0.7^{b} // 149.3 ± 1.1^{a}	62.2 ± 3.3^{b}
130 ºC	153.9 ± 0.1^{b}	57.4 ± 5.4^{a,b,c}	60.3 ± 1.9^{b}	38.1 ± 5.5^{a}	44.7 ± 0.3^{a}	9.8 ± 4.1^{b}	132.4 ± 0.7^{a,b} // 149.4 ± 0.3^{a}	60.5 ± 0.6^{b}
140 ºC	155.1 ± 0.2^{a,b}	58.1 ± 1.6^{a}	58.6 ± 1.5^{b}	39.6 ± 2.2^{a}	43.7 ± 1.3^{a}	6.4 ± 2.1^{a,b}	132.3 ± 1.2^{a,b} // 149.8 ± 0.8^{a}	59.6 ± 0.9^{b}
150 ºC	155.1 ± 0.8^{a,b}	53.6 ± 2.3^{c}	58.1 ± 0.3^{b}	40.4 ± 1.5^{a}	41.3 ± 4.8^{a,b}	9.6 ± 2.9^{b}	132.9 ± 0.1^{b} // 149.9 ± 0.4^{a}	60.3 ± 3.4^{a,b}

$^{a-c}$ Different letters in the same column indicate a significant difference among the samples ($p < 0.05$).

6. References

Acevedo, F., P. Villegas, V. Urtuvia, J. Hermosilla, R. Navia, and M. Seeger. 2018. "Bacterial polyhydroxybutyrate for electrospun fiber production." *International Journal of Biological Macromolecules* 106:692-697. doi: 10.1016/j.ijbiomac.2017.08.066.

Agüero, A., M. C. Morcillo, L. Quiles-Carrillo, R. Balart, T. Boronat, D. Lascano, S. Torres-Giner, and O. Fenollar. 2019. "Study of the influence of the reprocessing cycles on the final properties of polylactide pieces obtained by injection molding." *Polymers* 11 (12). doi: 10.3390/polym11121908.

Albuquerque, M. G. E., C. A. V. Torres, and M. A. M. Reis. 2010. "Polyhydroxyalkanoate (PHA) production by a mixed microbial culture using sugar molasses: Effect of the influent substrate concentration on culture selection." *Water Research* 44 (11):3419-3433. doi: 10.1016/j.watres.2010.03.021.

Ali Dadfar, S. M., I. Alemzadeh, S. M. Reza Dadfar, and M. Vosoughi. 2011. "Studies on the oxygen barrier and mechanical properties of low density polyethylene/organoclay nanocomposite films in the presence of ethylene vinyl acetate copolymer as a new type of compatibilizer." *Materials and Design* 32 (4):1806-1813. doi: 10.1016/j.matdes.2010.12.028.

Alp-Erbay, E., K. J. Figueroa-Lopez, J. M. Lagaron, E. Çağlak, and S. Torres-Giner. 2019. "The impact of electrospun films of poly(ε-caprolactone) filled with nanostructured zeolite and silica microparticles on in vitro histamine formation by Staphylococcus aureus and Salmonella Paratyphi A." *Food Packaging and Shelf Life* 22. doi: 10.1016/j.fpsl.2019.100414.

Arfat, Y. A., J. Ahmed, N. Hiremath, R. Auras, and A. Joseph. 2017. "Thermo-mechanical, rheological, structural and antimicrobial properties of bionanocomposite films based on fish skin gelatin and silver-copper nanoparticles." *Food Hydrocolloids* 62:191-202. doi: 10.1016/j.foodhyd.2016.08.009.

Castro-Mayorga, J. L., M. J. Fabra, and J. M. Lagaron. 2016. "Stabilized nanosilver based antimicrobial poly(3-hydroxybutyrate-co-3-hydroxyvalerate) nanocomposites of interest in active food packaging." *Innovative Food Science and Emerging Technologies* 33:524-533. doi: 10.1016/j.ifset.2015.10.019.

Castro Mayorga, J. L., M. J. Fabra Rovira, L. Cabedo Mas, G. Sánchez Moragas, and J. M. Lagarón Cabello. 2018. "Antimicrobial nanocomposites and electrospun coatings based on poly(3-hydroxybutyrate-co-3-hydroxyvalerate) and copper oxide nanoparticles for active packaging and coating applications." *Journal of Applied Polymer Science* 135 (2). doi: 10.1002/app.45673.

Cherpinski, A., M. Gozutok, H. T. Sasmazel, S. Torres-Giner, and J. M. Lagaron. 2018. "Electrospun oxygen scavenging films of poly(3-hydroxybutyrate) containing palladium nanoparticles for active packaging applications." *Nanomaterials* 8 (7). doi: 10.3390/nano8070469.

Cherpinski, A., S. Torres-Giner, L. Cabedo, and J. M. Lagaron. 2017. "Post-processing optimization of electrospun submicron poly(3-hydroxybutyrate) fibers to obtain continuous films of interest in food packaging applications." *Food Additives and Contaminants - Part A Chemistry, Analysis, Control, Exposure and Risk Assessment* 34 (10):1817-1830. doi: 10.1080/19440049.2017.1355115.

Cherpinski, A., S. Torres-Giner, L. Cabedo, J. A. Méndez, and J. M. Lagaron. 2018. "Multilayer structures based on annealed electrospun biopolymer coatings of interest in water and aroma barrier fiber-based food packaging applications." *Journal of Applied Polymer Science* 135 (24). doi: 10.1002/app.45501.

Cherpinski, A., S. Torres-Giner, J. Vartiainen, M. S. Peresin, P. Lahtinen, and J. M. Lagaron. 2018. "Improving the water resistance of nanocellulose-based films with polyhydroxyalkanoates processed by the electrospinning coating technique." *Cellulose* 25 (2):1291-1307. doi: 10.1007/s10570-018-1648-z.

Choi, J. I., and S. Y. Lee. 1997. "Process analysis and economic evaluation for poly(3-hydroxybutyrate) production by fermentation." *Bioprocess Engineering* 17 (6):335-342. doi: 10.1007/s004490050394.

Coats, E. R., F. J. Loge, M. P. Wolcott, K. Englund, and A. G. McDonald. 2007. "Synthesis of polyhydroxyalkanoates in municipal wastewater treatment." *Water Environment Research* 79 (12):2396-2403. doi: 10.2175/106143007X183907.

Colombo, B., T. P. Sciarria, M. Reis, B. Scaglia, and F. Adani. 2016. "Polyhydroxyalkanoates (PHAs) production from fermented cheese whey by using a mixed microbial culture." *Bioresource Technology* 218:692-699. doi: 10.1016/j.biortech.2016.07.024.

Dionisi, D., G. Carucci, M. Petrangeli Papini, C. Riccardi, M. Majone, and F. Carrasco. 2005. "Olive oil mill effluents as a feedstock for production of biodegradable polymers." *Water Research* 39 (10):2076-2084. doi: 10.1016/j.watres.2005.03.011.

Doshi, J., and D. H. Reneker. 1995. "Electrospinning process and applications of electrospun fibers." *Journal of Electrostatics* 35 (2-3):151-160. doi: 10.1016/0304-3886(95)00041-8.

Fabra, M. J., A. Lopez-Rubio, and J. M. Lagaron. 2014. "Nanostructured interlayers of zein to improve the barrier properties of high barrier polyhydroxyalkanoates and other polyesters." *Journal of Food Engineering* 127:1-9. doi: 10.1016/j.jfoodeng.2013.11.022.

Fernández-Dacosta, C., J. A. Posada, R. Kleerebezem, M. C. Cuellar, and A. Ramirez. 2015. "Microbial community-based polyhydroxyalkanoates (PHAs) production from wastewater: Techno-economic analysis and ex-ante environmental assessment." *Bioresource Technology* 185:368-377. doi: 10.1016/j.biortech.2015.03.025.

Figueroa-Lopez, K. J., A. A. Vicente, M. A. M. Reis, S. Torres-Giner, and J. M. Lagaron. 2019. "Antimicrobial and antioxidant performance of various essential oils and natural extracts and their incorporation into biowaste derived poly(3-hydroxybutyrate-co-3-hydroxyvalerate) layers made from electrospun ultrathin fibers." *Nanomaterials* 9 (2). doi: 10.3390/nano9020144.

Fiorese, M. L., F. Freitas, J. Pais, A. M. Ramos, G. M. F. De Aragão, and M. A. M. Reis. 2009. "Recovery of polyhydroxybutyrate (PHB) from Cupriavidus necator biomass by solvent extraction with 1,2-propylene carbonate." *Engineering in Life Sciences* 9 (6):454-461. doi: 10.1002/elsc.200900034.

Griffin, G. J. L. 1994. Chemistry and technology of biodegradable polymers. edited by G. J. L. Griffin. London.: Blackie Academic & Professional

Gurieff, N., and P. Lant. 2007. "Comparative life cycle assessment and financial analysis of mixed culture polyhydroxyalkanoate production." *Bioresource Technology* 98 (17):3393-3403. doi: 10.1016/j.biortech.2006.10.046.

Harini, K., and M. Sukumar. 2019. "Development of cellulose-based migratory and nonmigratory active packaging films." *Carbohydrate Polymers* 204:202-213. doi: 10.1016/j.carbpol.2018.10.018.

Hassan, M. A., Y. Shirai, N. Kusubayashi, M. I. A. Karim, K. Nakanishi, and K. Hashimoto. 1997. "The production of polyhydroxyalkanoate from anaerobically treated palm oil mill effluent by Rhodobacter sphaeroides." *Journal of Fermentation and Bioengineering* 83 (5):485-488. doi: 10.1016/S0922-338X(97)83007-3.

Hu, M., C. Li, X. Li, M. Zhou, J. Sun, F. Sheng, S. Shi, and L. Lu. 2018. "Zinc oxide/silver bimetallic nanoencapsulated in PVP/PCL nanofibres for improved antibacterial activity." *Artificial Cells, Nanomedicine and Biotechnology* 46 (6):1248-1257. doi: 10.1080/21691401.2017.1366339.

Jung, H. R., T. R. Choi, Y. H. Han, Y. L. Park, J. Y. Park, H. S. Song, S. Y. Yang, S. K. Bhatia, R. Gurav, H. Park, S. Namgung, K. Y. Choi, and Y. H. Yang. 2020. "Production of blue-colored polyhydroxybutyrate (PHB) by one-pot production and coextraction of indigo and PHB from recombinant Escherichia coli." *Dyes and Pigments* 173. doi: 10.1016/j.dyepig.2019.107889.

Kanatt, S. R., M. S. Rao, S. P. Chawla, and A. Sharma. 2012. "Active chitosan-polyvinyl alcohol films with natural extracts." *Food Hydrocolloids* 29 (2):290-297. doi: 10.1016/j.foodhyd.2012.03.005.

Koller, M. 2014. "Poly(hydroxyalkanoates) for food packaging: Application and attempts towards implementation." *Applied Food Biotechnology* 1 (1):3-15. doi: 10.22037/afb.v1i1.7127.

Koller, M., L. Maršálek, M. M. de Sousa Dias, and G. Braunegg. 2017. "Producing microbial polyhydroxyalkanoate (PHA) biopolyesters in a sustainable manner." *New Biotechnology* 37:24-38. doi: 10.1016/j.nbt.2016.05.001.

Korkakaki, E., M. Mulders, A. Veeken, R. Rozendal, M. C. M. van Loosdrecht, and R. Kleerebezem. 2016. "PHA production from the organic fraction of municipal solid waste (OFMSW): Overcoming the inhibitory matrix." *Water Research* 96:74-83. doi: 10.1016/j.watres.2016.03.033.

Kourmentza, C., and M. Kornaros. 2016. "Biotransformation of volatile fatty acids to polyhydroxyalkanoates by employing mixed microbial consortia: The effect of pH and carbon source." *Bioresource Technology* 222:388-398. doi: 10.1016/j.biortech.2016.10.014.

Kunasundari, B., and K. Sudesh. 2011. "Isolation and recovery of microbial polyhydroxyalkanoates." *Express Polymer Letters* 5 (7):620-634. doi: 10.3144/expresspolymlett.2011.60.

Lagarón, J. M. 2011. "Multifunctional and nanoreinforced polymers for food packaging." In *Multifunctional and Nanoreinforced Polymers for Food Packaging*, 1-28.

Lasprilla-Botero, J., S. Torres-Giner, M. Pardo-Figuerez, M. álvarez-Láinez, and J. M. Lagaron. 2018. "Superhydrophobic bilayer coating based on annealed electrospun ultrathin poly(ε-caprolactone) fibers and electrosprayed nanostructured silica microparticles for easy emptying packaging applications." *Coatings* 8 (5). doi: 10.3390/coatings8050173.

Laycock, B., P. Halley, S. Pratt, A. Werker, and P. Lant. 2013. "The chemomechanical properties of microbial polyhydroxyalkanoates." *Progress in Polymer Science* 38 (3-4):536-583. doi: 10.1016/j.progpolymsci.2012.06.003.

Li, L., W. Huang, B. Wang, W. Wei, Q. Gu, and P. Chen. 2015. "Properties and structure of polylactide/poly (3-hydroxybutyrate-co-3-hydroxyvalerate) (PLA/PHBV) blend fibers." *Polymer* 68:183-194. doi: 10.1016/j.polymer.2015.05.024.

Madkour, M. H., D. Heinrich, M. A. Alghamdi, I. I. Shabbaj, and A. Steinbüchel. 2013. "PHA recovery from biomass." *Biomacromolecules* 14 (9):2963-2972. doi: 10.1021/bm4010244.

Mata-Alvarez, J., J. Dosta, M. S. Romero-Güiza, X. Fonoll, M. Peces, and S. Astals. 2014. "A critical review on anaerobic co-digestion achievements between 2010 and 2013." *Renewable and Sustainable Energy Reviews* 36:412-427. doi: 10.1016/j.rser.2014.04.039.

Melendez-Rodriguez, B., J. L. Castro-Mayorga, M. A. M. Reis, C. Sammon, L. Cabedo, S. Torres-Giner, and J. M. Lagaron. 2018. "Preparation and Characterization of Electrospun Food Biopackaging Films of Poly(3-hydroxybutyrate-co-3-hydroxyvalerate) Derived From Fruit Pulp Biowaste." *Frontiers in Sustainable Food Systems* 2. doi: 10.3389/fsufs.2018.00038.

Melendez-Rodriguez, B., K. J. Figueroa-Lopez, A. Bernardos, R. Martínez-Máñez, L. Cabedo, S. Torres-Giner, and J. M. Lagaron. 2019. "Electrospun antimicrobial films of poly(3-hydroxybutyrate-co-3-hydroxyvalerate) containing eugenol essential oil encapsulated in mesoporous silica nanoparticles." *Nanomaterials* 9 (2). doi: 10.3390/nano9020227.

Melendez-Rodriguez, B., S. Torres-Giner, A. Aldureid, L. Cabedo, and J. M. Lagaron. 2019. "Reactive melt mixing of poly(3-hydroxybutyrate)/rice husk flour composites with purified biosustainably produced poly(3-hydroxybutyrate-co-3-hydroxyvalerate)." *Materials* 12 (13). doi: 10.3390/ma12132152.

Morgan-Sagastume, F., M. Hjort, D. Cirne, F. Gérardin, S. Lacroix, G. Gaval, L. Karabegovic, T. Alexandersson, P. Johansson, A. Karlsson, S. Bengtsson, M. V. Arcos-Hernández, P. Magnusson, and A. Werker. 2015. "Integrated production of polyhydroxyalkanoates (PHAs) with municipal wastewater and sludge treatment at pilot scale." *Bioresource Technology* 181:78-89. doi: 10.1016/j.biortech.2015.01.046.

Pal, Kunal, Ajit Banthia, and Dipak K. Majumdar. 2009. "Polymeric Hydrogels: Characterization and Biomedical Applications." *Designed Monomers & Polymers,VSP, an imprint of Brill* 12:197-220. doi: 10.1163/156855509X436030.

Panaitescu, D. M., C. A. Nicolae, A. N. Frone, I. Chiulan, P. O. Stanescu, C. Draghici, M. Iorga, and M. Mihailescu. 2017. "Plasticized poly(3-hydroxybutyrate) with improved melt processing and balanced properties." *Journal of Applied Polymer Science* 134 (19). doi: 10.1002/app.44810.

Quiles-Carrillo, L., N. Montanes, J. M. Lagaron, R. Balart, and S. Torres-Giner. 2019a. "Bioactive multilayer polylactide films with controlled release capacity of gallic acid accomplished by incorporating electrospun nanostructured coatings and interlayers." *Applied Sciences (Switzerland)* 9 (3). doi: 10.3390/app9030533.

Quiles-Carrillo, L., N. Montanes, J. M. Lagaron, R. Balart, and S. Torres-Giner. 2019b. "In Situ Compatibilization of Biopolymer Ternary Blends by Reactive Extrusion with Low-Functionality Epoxy-Based Styrene–Acrylic Oligomer." *Journal of Polymers and the Environment* 27 (1):84-96. doi: 10.1007/s10924-018-1324-2.

Rehm, B. H. A. 2003. "Polyester synthases: Natural catalysts for plastics." *Biochemical Journal* 376 (1):15-33. doi: 10.1042/BJ20031254.

Reis, M., M. Albuquerque, M. Villano, and M. Majone. 2011. "Mixed Culture Processes for Polyhydroxyalkanoate Production from Agro-Industrial Surplus/Wastes as Feedstocks." In *Comprehensive Biotechnology, Second Edition*, 669-683.

Riekel, C., M. C. G. Gutiérrez, A. Gourrier, and S. Roth. 2003. "Recent synchrotron radiation microdiffraction experiments on polymer and biopolymer fibers." *Analytical and Bioanalytical Chemistry* 376 (5):594-601. doi: 10.1007/s00216-003-1976-0.

Saharan, B. S., A. Grewal, and P. Kumar. 2014. "Biotechnological production of polyhydroxyalkanoates: a review on trends and latest developments." *Chin. J. Biol.* 2014:1-18.

Sanchez-Garcia, M. D., E. Gimenez, and J. M. Lagaron. 2007. "Novel PET nanocomposites of interest in food packaging applications and comparative barrier performance with biopolyester nanocomposites." *Journal of Plastic Film and Sheeting* 23 (2):133-148. doi: 10.1177/8756087907083590.

Sanchez-Garcia, M. D., E. Gimenez, and J. M. Lagaron. 2008. "Morphology and barrier properties of solvent cast composites of thermoplastic biopolymers and purified cellulose fibers." *Carbohydrate Polymers* 71 (2):235-244. doi: 10.1016/j.carbpol.2007.05.041.

Sängerlaub, S., M. Brüggemann, N. Rodler, V. Jost, and K. D. Bauer. 2019. "Extrusion coating of paper with poly(3-hydroxybutyrate-co-3-hydroxyvalerate) (PHBV)-Packaging related functional properties." *Coatings* 9 (7). doi: 10.3390/coatings9070457.

Sato, H., N. Suttiwijitpukdee, T. Hashimoto, and Y. Ozaki. 2012. "Simultaneous synchrotron SAXS/WAXD study of composition fluctuations, cold-crystallization, and melting in biodegradable polymer blends of cellulose acetate butyrate and poly(3-hydroxybutyrate)." *Macromolecules* 45 (6):2783-2795. doi: 10.1021/ma202606y.

Shibata, M., S. Oyamada, S. I. Kobayashi, and D. Yaginuma. 2004. "Mechanical properties and biodegradability of green composites based on biodegradable polyesters and lyocell fabric." *Journal of Applied Polymer Science* 92 (6):3857-3863. doi: 10.1002/app.20405.

Shiku, Y., P. Y. Hamaguchi, S. Benjakul, W. Visessanguan, and M. Tanaka. 2004. "Effect of surimi quality on properties of edible films based on Alaska pollack." *Food Chemistry* 86 (4):493-499. doi: 10.1016/j.foodchem.2003.09.022.

Škrbić, Ž, and V. Divjaković. 1996. "Temperature influence on changes of parameters of the unit cell of biopolymer PHB." *Polymer* 37 (3):505-507. doi: 10.1016/0032-3861(96)82922-3.

Spagnol, C., E. H. Fragal, A. G. B. Pereira, C. V. Nakamura, E. C. Muniz, H. D. M. Follmann, R. Silva, and A. F. Rubira. 2018. "Cellulose nanowhiskers decorated with silver nanoparticles as an additive to antibacterial polymers membranes fabricated by electrospinning." *Journal of Colloid and Interface Science* 531:705-715. doi: 10.1016/j.jcis.2018.07.096.

Tanpichai, S., S. Witayakran, J. Wootthikanokkhan, Y. Srimarut, W. Woraprayote, and Y. Malila. 2020. "Mechanical and antibacterial properties of the chitosan coated cellulose paper for packaging applications: Effects of molecular weight types and concentrations of chitosan." *International Journal of Biological Macromolecules* 155:1510-1519. doi: 10.1016/j.ijbiomac.2019.11.128.

Thomas, S., and P. M. Visakh. 2011. "Engineering and Specialty Thermoplastics: Polyethers and Polyesters: State-of-the-art, New Challenges and Opportunities." In *Handbook of Engineering and Speciality Thermoplastics: Polyethers and Polyesters*, 1-14.

Torres-Giner, S., J. V. Gimeno-Alcañiz, M. J. Ocio, and J. M. Lagaron. 2011. "Optimization of electrospun polylactide-based ultrathin fibers for osteoconductive bone scaffolds." *Journal of Applied Polymer Science* 122 (2):914-925. doi: 10.1002/app.34208.

Torres-Giner, S., L. Hilliou, B. Melendez-Rodriguez, K. J. Figueroa-Lopez, D. Madalena, L. Cabedo, J. A. Covas, A. A. Vicente, and J. M. Lagaron. 2018. "Melt processability, characterization, and antibacterial activity of compression-molded green composite sheets made of poly(3-hydroxybutyrate-co-3-hydroxyvalerate) reinforced with coconut

fibers impregnated with oregano essential oil." *Food Packaging and Shelf Life* 17:39-49. doi: 10.1016/j.fpsl.2018.05.002.

Torres-Giner, S., N. Montanes, T. Boronat, L. Quiles-Carrillo, and R. Balart. 2016. "Melt grafting of sepiolite nanoclay onto poly(3-hydroxybutyrate-co-4-hydroxybutyrate) by reactive extrusion with multi-functional epoxy-based styrene-acrylic oligomer." *European Polymer Journal* 84:693-707. doi: 10.1016/j.eurpolymj.2016.09.057.

Torres-Giner, S., N. Montanes, V. Fombuena, T. Boronat, and L. Sanchez-Nacher. 2018. "Preparation and characterization of compression-molded green composite sheets made of poly(3-hydroxybutyrate) reinforced with long pita fibers." *Advances in Polymer Technology* 37 (5):1305-1315. doi: 10.1002/adv.21789.

Torres-Giner, S., S. Wilkanowicz, B. Melendez-Rodriguez, and J. M. Lagaron. 2017. "Nanoencapsulation of Aloe vera in Synthetic and Naturally Occurring Polymers by Electrohydrodynamic Processing of Interest in Food Technology and Bioactive Packaging." *Journal of Agricultural and Food Chemistry* 65 (22):4439-4448. doi: 10.1021/acs.jafc.7b01393.

Vahabi, H., L. Michely, G. Moradkhani, V. Akbari, M. Cochez, C. Vagner, E. Renard, M. R. Saeb, and V. Langlois. 2019. "Thermal stability and flammability behavior of poly(3-hydroxybutyrate) (PHB) based composites." *Materials* 12 (14). doi: 10.3390/ma12142239.

Valentino, F., G. Moretto, L. Lorini, D. Bolzonella, P. Pavan, and M. Majone. 2019. "Pilot-Scale Polyhydroxyalkanoate Production from Combined Treatment of Organic Fraction of Municipal Solid Waste and Sewage Sludge." *Industrial and Engineering Chemistry Research* 58 (27):12149-12158. doi: 10.1021/acs.iecr.9b01831.

Zhang, K., M. Misra, and A. K. Mohanty. 2014. "Toughened sustainable green composites from poly(3-hydroxybutyrate-co-3-hydroxyvalerate) based ternary blends and miscanthus biofiber." *ACS Sustainable Chemistry and Engineering* 2 (10):2345-2354. doi: 10.1021/sc500353v.

Zhang, M., H. Wu, and H. Chen. 2014. "Coupling of polyhydroxyalkanoate production with volatile fatty acid from food wastes and excess sludge." *Process Safety and Environmental Protection* 92 (2):171-178. doi: 10.1016/j.psep.2012.12.002.